

Supporting Information for:

Charge Carrier Resolved Relaxation of the First Excitonic State in CdSe Quantum Dots Probed with Near-Infrared Transient Absorption Spectroscopy

Eric A. McArthur, Adam J. Morris-Cohen, Kathryn E. Knowles, and Emily A. Weiss*

Department of Chemistry, Northwestern University, 2145 Sheridan Rd., Evanston, IL 60208-3113

*corresponding author. Email: e-weiss@northwestern.edu

EXPERIMENTAL DETAILS

UV-Vis Absorption. Ground state absorption measurements, Figure S1, were performed on a Varian Cary 5000 using a 2-mm pathlength quartz cell. The baselines of all spectra were corrected with neat solvent prior to measurement.

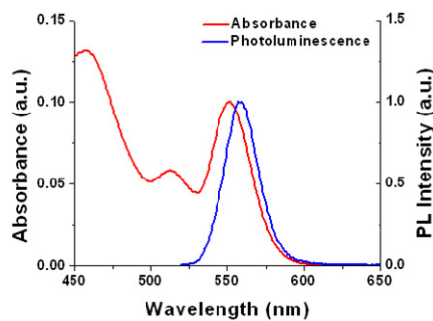


Figure S1. Ground state absorption spectrum (red) and photoluminescence emission spectrum (blue) of 5×10^{-6} M 4.1-nm CdSe QDs in CCl_4 .

Steady State Photoluminescence (PL). Steady state PL spectra, Figure S1, were collected on a Horiba Fluorolog-3 spectrofluorometer. Samples were excited with 509 nm light with

excitation slit width set to a 1-nm effective bandwidth. Emission was collected in a right-angle geometry with a photomultiplier tube from 512 nm – 850 nm with the emission slit width set to a 1-nm effective bandwidth.

Inductively Coupled Plasma-Atomic Emission Spectroscopy (ICP-AES). Approximately 25 nmoles of CdSe QD reference sample (no added ligand) dispersed in CCl₄ was dried with a stream of N₂(g) in 25-ml scintillation vial. Room temperature aqua regia (concentrated HCl: glacial HNO₃, 3:1 v/v) was added to the vial, and the undisturbed sample was digested over a period of one hour. The digested solution was diluted in μ -pore-filtered water to a concentration of 5% aqua regia and 8-9 μ g/ml Cd and 1-2 μ g/ml Se. The instrument was calibrated with ICP standards Cd²⁺ and Se²⁻ (1,000 μ g/ml in 2% HNO₃, Aldrich) diluted to concentrations of 2-10 μ g/ml in 5% HNO₃.

Spot Size Measurement and Calculation of the Expected Excited State Population, $\langle N \rangle$.

Spot size was measured prior to all TA measurements and power was adjusted as necessary to maintain a population of $\langle N \rangle = 0.1$ in the first excitonic state of the QDs. The transverse profile of the pump beam was first examined using a CMOS camera (Thor Labs) equipped with a 1000:1 neutral density filter to verify pump beam was operating in the fundamental TEM₀₀ mode. At the position of the sample the beam spot sizes were measured by translating a blade attached to a manual translation stage perpendicularly across the beam. A micrometer was used to record the translated distance while recording the transmitted power using a UV enhanced Silicon photodetector (Newport). Transmitted power plotted against translated distance, Figure S2, reflects the power distribution of the transverse intensity profile of the beam, which is then fit to an error function to extract a spot size. The spot size is defined as the gaussian FWHM in our experiment.

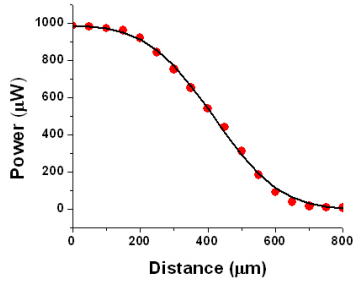


Figure S2. Transmitted power (red dots) versus blade translation distance fit to an error function (black) used to extract spot size.

Photon flux is then determined based on spot size measurements and used to calculate expected excited state occupation. This value is corrected for attenuation based on the approach of previous authors, eq 1.¹ In eq 1, $\langle N \rangle$ is the expectation value for excited state

$$\langle N \rangle = \frac{1000I_o}{N_a \ell c} (1 - \text{Exp}[-\ln(10)\varepsilon\ell c]) \quad (1)$$

QDs, I_o is the photon flux, N_a is Avagadro's number, ℓ is pathlength, ε is molar absorptivity, and c is concentration of QD.

NIR Continuum Probe Generation. A single filament continuum was generated in 1.2-cm thick sapphire plate and filtered with an 850-nm long wavepass filter to isolate the NIR wavelengths. The continuum was measured using a 256 pixel InGaAs linear array diode detector (Ultrafast Systems), Figure S3.

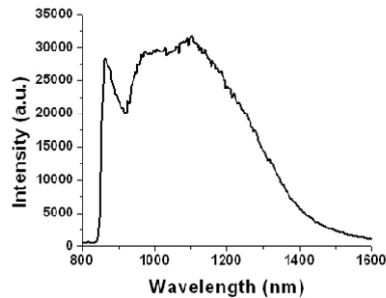


Figure S3. Near-infrared continuum generated in a sapphire plate for use as the probe in the TA experiment.

Shift of Optical Bandgap in the Presence of Octanethiol. At high QD surface coverage of OT (OT:QD = 70,000:1) the optical bandgap exhibits a 12 meV bathochromic shift (550 nm to 553 nm) due to tight binding of the sulfur head group to the surface Cd²⁺, Figure S4.

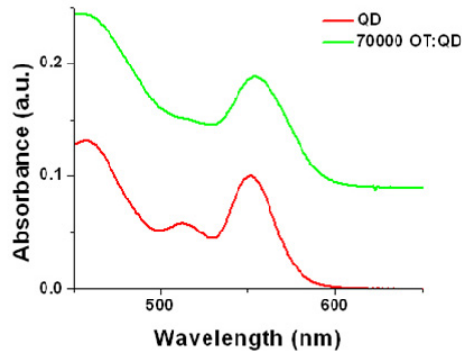


Figure S4. Ground state absorption spectrum of 5×10^{-6} M 4.1-nm CdSe QDs in CCl₄ native ligands (red) and 70000 OT:QD (green).

Calculation of the Driving Force for Electron Transfer from the CdSe QD to Benzoquinone (BQ). We estimated the driving force for eT from the QD to BQ, $\Delta G_{eT} = -E_{ES} + E_{IP}$, using Weller's expression based on the Born dielectric continuum model² of the solvent to determine the energy of formation of an ion pair, E_{IP} , in a solvent of arbitrary polarity, and E_{ES} (QD) = 2.2 eV.

$$E_{IP} = E_{ox} - E_{red} - \frac{e^2}{r_{DA}\epsilon_s} + e^2 \left(\frac{1}{2r_1} + \frac{1}{2r_2} \right) \left(\frac{1}{\epsilon_s} - \frac{1}{\epsilon_{sp}} \right) \quad (S1)$$

where E_{ox} ($\sim +1.0$ vs. SCE for the QD^{3,4}) and E_{red} ($= -0.41$ vs. SCE for BQ⁵) are, respectively, the oxidation and reduction potentials of the donor and acceptor in a high polarity solvent with dielectric constant ϵ_{sp} ($\epsilon_{sp} = 37.5$ for acetonitrile used here), e is the charge of the electron, r_1 and r_2 are the ionic radii of the radical ions (0.32 nm for BQ⁶), r_{DA} is the donor-acceptor distance), and ϵ_s is the static dielectric constant of the solvent in which the spectroscopy is performed ($\epsilon_s = 2.24$ for CCl₄ used here). The ionic radius of the QD and the donor-acceptor distance r_{DA} are not straightforward to estimate. According to Lifshitz, et al.⁷, who measured the anisotropic exchange interactions of electron-hole pairs in CdSe QDs using optically detected magnetic resonance, there exists “an ensemble of e-h pair distances, most probably around the periphery of a nanoparticle”, and “distribution of this value is limited by the size of the nanoparticles.” Assuming that the ion pair is an electron trapped on BQ and a hole trapped on the surface of the QD, and assuming that the hole traps on the same hemisphere of the QD as is located BQ, the average distance between electron and hole on the surface of a QD with radius of 2.05 nm is ~ 1.6 nm. If we assume that the ionic radius of the hole is equivalent to the radius of the QD = 2.05 nm (i.e., the delocalization of the hole is limited only by the spatial confinement of the QD lattice), then, using eq S1, $E_{IP} = 2.1$, and $\Delta G_{eT} = -0.1$ eV.

Global Analysis Representative Fits and Amplitude Parameters. Figure S5 shows representative fits of the TA data at 900 nm, 1074 nm, and 1249 nm probe wavelengths for QD reference samples (QDs with native ligands), and the associated residuals. Tables S1 – S5 contain the relative amplitudes (scaled such that total amplitude = 1) at each wavelength included in the global analysis for each QD-ligand sample used in the 1-octanethiol study. Tables S6 –

S11 contain the relative amplitude data for each QD-ligand sample used in the 1,4-benzoquinone study.

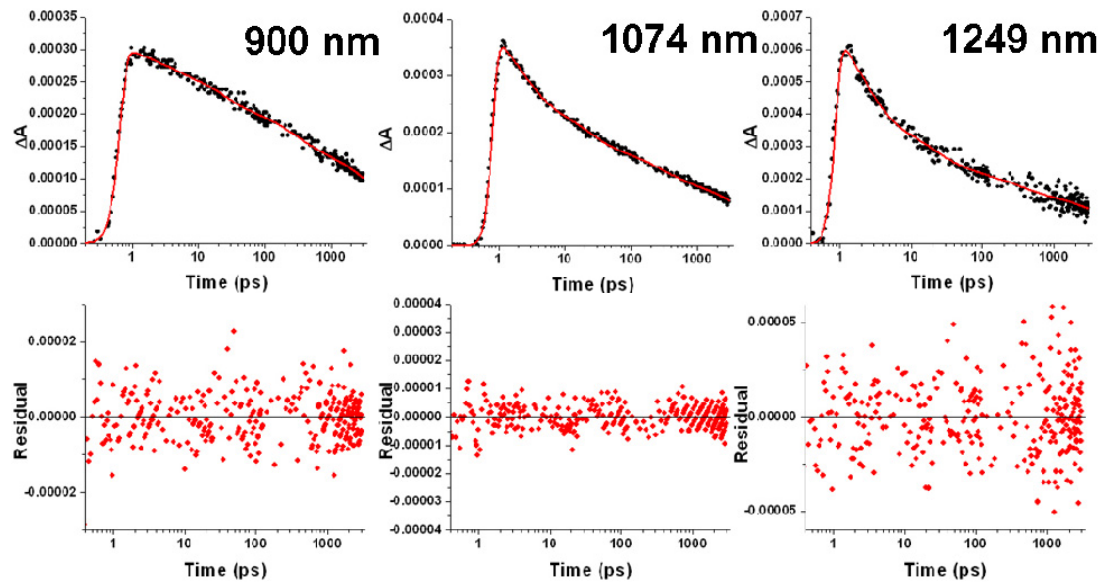


Figure S5. Representative fits of TA data and corresponding residuals for 900 nm, 1074 nm, and 1249 nm probe wavelengths for 4.1-nm CdSe QDs photoexcited with 550 nm pump light.

Uniqueness of the Global Fit. The uniqueness of the four exponential global fit⁸ is investigated by examining the statistical scatter of the independent parameters extracted from convergent fits based on a wide range of initial values. Additionally, covariance plots for each time constant shows steep distinct error wells that are consistent with the statistical scatter of the independent parameters.

Figure S6, below, shows the statistical scatter of the time constants based on a large

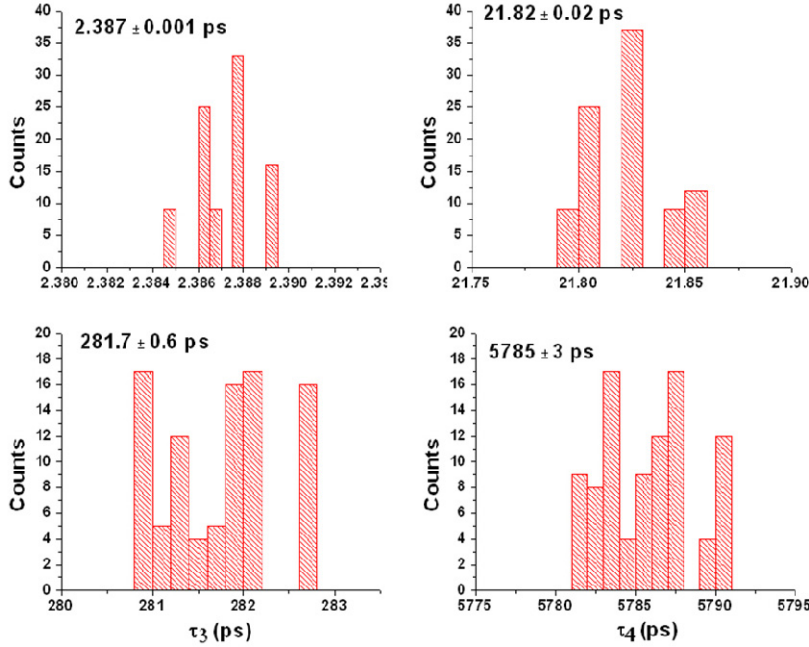


Figure S6. Representative statistical scatter for of the four time constants.

range of initial values (0.1 ps - 10000 ps for the time constants and 0.0003 - 0.001 for the amplitudes). It was found that, in general, most initial values led to fits that converge with uniform scattering of the residuals across a zero line. However, in the cases of some very extreme initial values the fit becomes trapped into a local minimum that corresponds to time constants and amplitudes that are unphysical and also exhibit grossly unacceptable curvature in the residual scatter. On the basis of these observations, we exclude these values from the statistics. For all four time constants and amplitudes, the statistical error is well below 1% relative error. This result confirms that the fits repeatedly converge to the same minima; therefore, the error wells are sufficiently steep and distinct and our fit is adequately unique. The uniqueness and small statistical error for both the amplitudes and time constants indicates that the experimentally determined standard deviation of the time constants, constructed from the

measurement of several different samples, is due to the heterogeneity of the QD ensemble, and batch-to-batch variation, and is not an artifact of the fitting process.

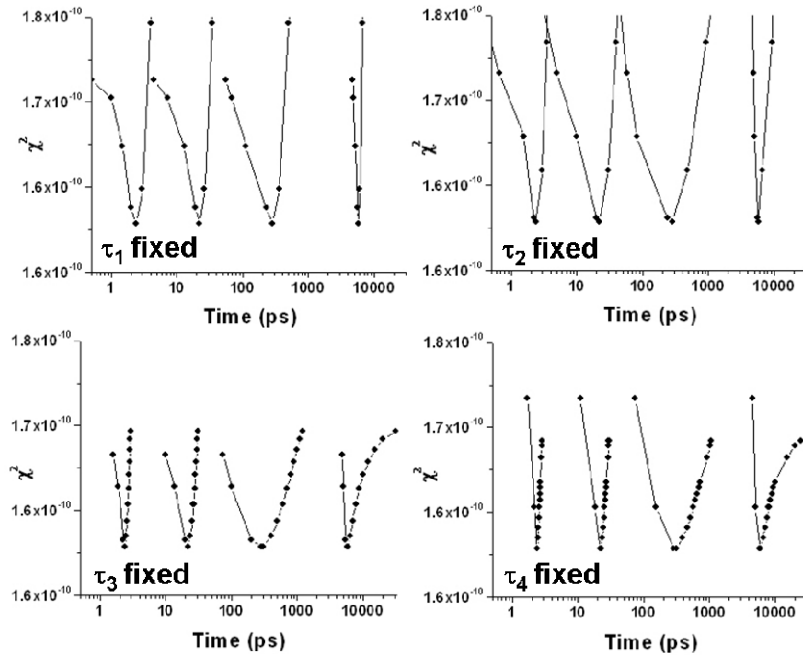


Figure S7. Reduced χ^2 error versus covariance of the individual time constants.

Figure S7 show the covariance for each of the four time constants. Each plot is constructed by fixing one time constant and allowing the fit to converge by adjusting forcing the other time constants. This procedure is then repeated for a small range of values for the fixed time constant. The plots display a small sampling of the reduced χ^2 error surface, which allows us to visualize the convergence minima and confirm that the minima are distinct.

Spectral Fits and Time Evolution of NIRTA Spectra. Figure S8 shows eight temporal slices of the NIR TA spectra of the QDs with their native ligands, and with added BQ and OT. The fits to the spectra (solid lines) are the sums of the individual amplitude components obtained from the global fit.

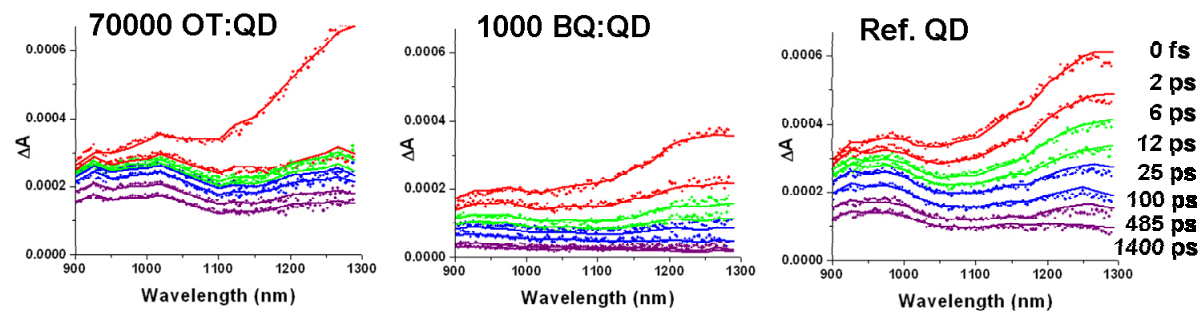


Figure S8. Time evolution of TA differential absorption spectra for 5×10^{-6} M 4.1-nm CdSe QDs in CCl_4 with native ligands, 1000 BQ:QD, and 70000 OT:QD.

Kinetics of the Recovery of the Ground State Bleach of QDs with their Native Ligands.

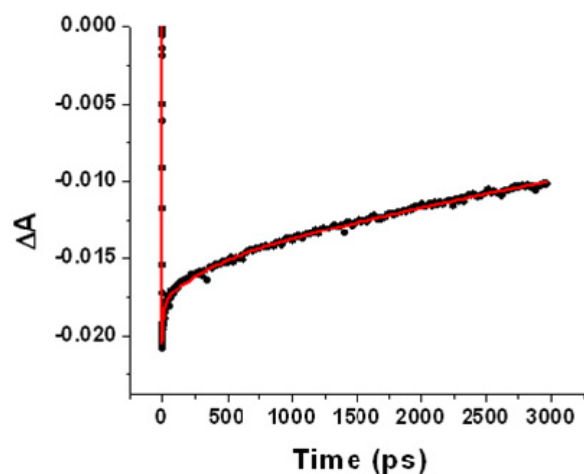


Figure S9. Visible TA dynamic at 561 nm probe wavelength for 5×10^{-6} M 4.1-nm CdSe QDs in CCl_4 with native ligands. The fit is a sum of an instrument response function and three exponential functions with time constants of 13.4 ps, 277 ps, and 6.3 ns.

Table S1. Amplitudes of Decay Components for QD Reference Sample (no added OT).

Wavelength (nm)	Spectral Amp.	Amp. (1.64 ps)	Amp. (22.02 ps)	Amp. (276.6 ps)	Amp. (6243 ps)
898	0.000287	0.12	0.24	0.25	0.40
926	0.000318	0.13	0.25	0.24	0.39
950	0.000298	0.14	0.25	0.22	0.38
974	0.000315	0.18	0.24	0.22	0.36
1002	0.000312	0.21	0.25	0.21	0.33
1022	0.000315	0.25	0.25	0.20	0.30
1050	0.000325	0.30	0.25	0.18	0.28
1074	0.000345	0.32	0.25	0.17	0.26
1101	0.000380	0.35	0.25	0.17	0.24
1122	0.000423	0.35	0.25	0.15	0.24
1149	0.000471	0.38	0.25	0.14	0.23
1173	0.000530	0.40	0.24	0.15	0.22
1201	0.000619	0.40	0.25	0.14	0.21
1222	0.000630	0.41	0.24	0.14	0.21
1246	0.000627	0.42	0.25	0.14	0.20
1266	0.000633	0.42	0.24	0.13	0.21
1290	0.000618	0.43	0.23	0.13	0.21

Table S2. Amplitudes of Decay Components for Sample with OT:QD = 1:1.

Wavelength (nm)	Spectral Amplitude	Amplitude (1.20)	Amplitude (12.55)	Amplitude (160.9)	Amplitude (4792)
898	0.000310	0.12	0.20	0.27	0.41
926	0.000364	0.13	0.23	0.25	0.40
950	0.000335	0.13	0.24	0.25	0.38
974	0.000339	0.15	0.24	0.24	0.37
1002	0.000357	0.18	0.25	0.23	0.34
1019	0.000353	0.22	0.26	0.21	0.32
1050	0.000359	0.26	0.27	0.20	0.28
1070	0.000389	0.28	0.26	0.19	0.26
1101	0.000411	0.31	0.27	0.17	0.25
1118	0.000434	0.33	0.25	0.18	0.23
1149	0.000487	0.34	0.27	0.17	0.22
1170	0.000502	0.38	0.24	0.17	0.21
1201	0.000562	0.36	0.26	0.19	0.20
1222	0.000600	0.37	0.24	0.20	0.19
1249	0.000670	0.39	0.23	0.20	0.18
1266	0.000720	0.38	0.22	0.20	0.19
1294	0.000734	0.38	0.23	0.19	0.20

Table S3. Amplitudes of Decay Components for Sample with OT:QD = 10:1.

Wavelength (nm)	Spectral Amp.	Amp. (1.19 ps)	Amp. (7.32 ps)	Amp. (113.8 ps)	Amp. (4494 ps)
898	0.000262	0.03	0.19	0.28	0.50
926	0.000290	0.01	0.22	0.28	0.49
950	0.000274	0.02	0.24	0.27	0.47
974	0.000281	0.03	0.25	0.26	0.46
1002	0.000276	0.08	0.26	0.25	0.41
1022	0.000283	0.12	0.27	0.24	0.37
1050	0.000292	0.14	0.28	0.23	0.35
1074	0.000309	0.19	0.27	0.22	0.31
1101	0.000342	0.21	0.27	0.22	0.30
1122	0.000382	0.23	0.28	0.20	0.29
1149	0.000414	0.26	0.27	0.19	0.28

1173	0.000473	0.28	0.26	0.20	0.26
1201	0.000550	0.31	0.24	0.19	0.26
1222	0.000597	0.31	0.24	0.19	0.26
1249	0.000650	0.32	0.23	0.19	0.26
1266	0.000674	0.31	0.23	0.18	0.27
1294	0.000651	0.31	0.23	0.17	0.28

Table S4. Amplitudes of Decay Components for Sample with OT:QD = 1000:1.

Wavelength (nm)	Spectral Amp.	Amp. (0.421 ps)	Amp. (4.26 ps)	Amp. (78.8 ps)	Amp. (4393 ps)
901	0.000269	0.08	0.16	0.33	0.42
926	0.000294	0.03	0.20	0.34	0.44
950	0.000268	0.00	0.21	0.35	0.44
974	0.000281	0.00	0.23	0.34	0.43
1002	0.000278	0.02	0.26	0.33	0.39
1022	0.000292	0.04	0.29	0.32	0.35
1050	0.000313	0.09	0.31	0.29	0.31
1074	0.000336	0.11	0.33	0.27	0.29
1101	0.000365	0.13	0.35	0.25	0.28
1122	0.000412	0.16	0.35	0.24	0.25
1149	0.000470	0.18	0.36	0.23	0.23
1173	0.000525	0.21	0.36	0.21	0.22
1201	0.000631	0.22	0.36	0.21	0.21
1222	0.000670	0.21	0.38	0.20	0.21
1249	0.000742	0.24	0.36	0.19	0.20
1273	0.000748	0.23	0.37	0.19	0.21
1290	0.000730	0.21	0.38	0.19	0.21

Table S5. Amplitudes of Decay Components for Sample with OT:QD = 70000:1.

Wavelength (nm)	Spectral Amp.	Amp. (0.296 ps)	Amp. (3.80 ps)	Amp. (129.0 ps)	Amp. (5199 ps)
898	0.000295	0.35	0.05	0.07	0.53
926	0.000311	0.30	0.07	0.07	0.56
950	0.000319	0.37	0.05	0.07	0.51
974	0.000322	0.35	0.06	0.07	0.52
1002	0.000357	0.40	0.06	0.07	0.47
1019	0.000366	0.39	0.07	0.07	0.47
1050	0.000371	0.43	0.07	0.07	0.42
1067	0.000378	0.46	0.08	0.07	0.39
1101	0.000383	0.50	0.09	0.07	0.34
1122	0.000415	0.50	0.10	0.06	0.33
1149	0.000440	0.53	0.10	0.06	0.31
1170	0.000479	0.55	0.11	0.06	0.29
1201	0.000545	0.55	0.12	0.05	0.28
1218	0.000579	0.56	0.12	0.05	0.27
1249	0.000640	0.57	0.13	0.05	0.25
1266	0.000659	0.56	0.14	0.05	0.24
1290	0.000665	0.59	0.14	0.04	0.23

Table S6. Amplitudes of Decay Components for QD Reference Sample (no added BQ).

Wavelength (nm)	Spectral Amplitude	Amplitude (0.783)	Amplitude (17.57)	Amplitude (282.6)	Amplitude (5836)
898	0.000227	0.11	0.19	0.17	0.53
926	0.000272	0.13	0.20	0.16	0.51
950	0.000261	0.13	0.20	0.16	0.51
974	0.000286	0.13	0.21	0.16	0.50
1002	0.000294	0.17	0.22	0.14	0.47
1022	0.000294	0.23	0.23	0.14	0.40
1050	0.000287	0.29	0.25	0.12	0.34
1074	0.000309	0.32	0.25	0.11	0.31
1101	0.000333	0.32	0.28	0.10	0.30
1122	0.000369	0.33	0.28	0.09	0.30
1149	0.000414	0.35	0.29	0.09	0.28
1173	0.000454	0.35	0.29	0.09	0.27
1197	0.000493	0.37	0.30	0.07	0.26
1222	0.000537	0.36	0.31	0.07	0.25
1249	0.000556	0.37	0.32	0.06	0.26
1283	0.000515	0.35	0.34	0.06	0.25

Table S7. Amplitudes of Decay Components for Sample with BQ:QD = 1:1.

Wavelength (nm)	Spectral Amplitude	Amplitude (1.94)	Amplitude (20.25)	Amplitude (280.9)	Amplitude (7710)
898	0.000302	0.087	0.20	0.22	0.49
926	0.000358	0.11	0.19	0.22	0.48
950	0.000351	0.13	0.19	0.21	0.47
974	0.000367	0.14	0.19	0.21	0.46
1002	0.000364	0.17	0.20	0.19	0.43
1019	0.000357	0.22	0.21	0.19	0.39
1050	0.000355	0.28	0.21	0.17	0.33
1074	0.000375	0.31	0.22	0.16	0.31
1101	0.000389	0.33	0.22	0.16	0.29
1122	0.000420	0.34	0.22	0.15	0.29
1149	0.000466	0.36	0.23	0.14	0.28
1170	0.000486	0.38	0.22	0.15	0.25
1201	0.000563	0.39	0.23	0.13	0.25
1222	0.000605	0.39	0.24	0.13	0.25
1249	0.000648	0.40	0.23	0.13	0.24
1266	0.000662	0.40	0.23	0.13	0.24
1294	0.000662	0.39	0.23	0.13	0.25

Table S8. Amplitudes of Decay Components for Sample with BQ:QD = 10:1.

Wavelength (nm)	Spectral Amplitude	Amplitude (2.02)	Amplitude (21.58)	Amplitude (327.7)	Amplitude (5787)
898	0.000274	0.16	0.21	0.21	0.42
926	0.000333	0.16	0.19	0.19	0.46
950	0.000335	0.16	0.19	0.17	0.49
974	0.000357	0.17	0.20	0.16	0.47
1002	0.000365	0.20	0.20	0.15	0.45
1022	0.000363	0.26	0.21	0.14	0.40
1050	0.000355	0.31	0.21	0.13	0.35
1074	0.000377	0.33	0.22	0.12	0.33
1101	0.000408	0.37	0.22	0.12	0.29
1122	0.000432	0.39	0.22	0.12	0.27
1149	0.000479	0.41	0.23	0.11	0.25
1170	0.000516	0.43	0.23	0.10	0.24

Table S9. Amplitudes of Decay Components for Sample with BQ:QD = 100:1.

Wavelength (nm)	Spectral Amplitude	Amplitude (1.06)	Amplitude (8.26)	Amplitude (113.4)	Amplitude (4601)
898	0.000205	0.09	0.21	0.26	0.44
926	0.000255	0.10	0.21	0.24	0.44
950	0.000249	0.12	0.20	0.23	0.44
974	0.000273	0.12	0.23	0.23	0.42
1002	0.000272	0.16	0.23	0.22	0.39
1022	0.000268	0.22	0.23	0.21	0.34
1050	0.000271	0.24	0.26	0.20	0.30
1074	0.000284	0.28	0.25	0.20	0.27
1101	0.000301	0.29	0.27	0.19	0.25
1122	0.000331	0.33	0.26	0.18	0.23
1149	0.000366	0.34	0.28	0.17	0.22
1173	0.000389	0.34	0.30	0.16	0.20

Table S10. Amplitudes of Decay Components for Sample with BQ:QD = 1000:1.

Wavelength (nm)	Spectral Amplitude	Amplitude (1.27)	Amplitude (7.99)	Amplitude (161.1)	Amplitude (5292)
898	0.000186	0.26	0.28	0.25	0.21
926	0.000215	0.26	0.29	0.24	0.20
950	0.000218	0.28	0.31	0.23	0.17
974	0.000227	0.29	0.33	0.22	0.16
1002	0.000214	0.33	0.31	0.22	0.14
1019	0.000214	0.37	0.29	0.21	0.14
1050	0.000231	0.40	0.27	0.19	0.14
1070	0.000236	0.41	0.27	0.18	0.14
1101	0.000247	0.45	0.28	0.16	0.11
1122	0.000261	0.48	0.25	0.16	0.11
1149	0.000295	0.49	0.27	0.15	0.098
1173	0.000317	0.51	0.27	0.14	0.079
1201	0.000374	0.55	0.25	0.13	0.070
1218	0.000393	0.56	0.24	0.14	0.052
1249	0.000408	0.58	0.24	0.13	0.042
1266	0.000413	0.57	0.25	0.11	0.071
1290	0.000423	0.55	0.27	0.12	0.050

Table S11. Amplitudes of Decay Components for Sample with BQ:QD = 2500:1.

Wavelength (nm)	Spectral Amp.	Amp. (1.13 ps)	Amp. (6.98 ps)	Amp. (135.2 ps)	Amp. (5256 ps)
898	0.000182	0.26	0.29	0.26	0.19
926	0.000214	0.24	0.34	0.27	0.15
950	0.000207	0.26	0.35	0.24	0.15
974	0.000229	0.29	0.35	0.23	0.13
1002	0.000214	0.30	0.34	0.22	0.14
1022	0.000225	0.36	0.30	0.21	0.13
1050	0.000213	0.38	0.30	0.19	0.13
1074	0.000224	0.42	0.29	0.19	0.10
1101	0.000249	0.44	0.28	0.17	0.11
1118	0.000266	0.49	0.26	0.16	0.10
1153	0.000303	0.50	0.27	0.16	0.07
1173	0.000309	0.53	0.25	0.15	0.07
1201	0.000364	0.56	0.24	0.15	0.05
1222	0.000374	0.58	0.22	0.15	0.05
1246	0.000385	0.58	0.23	0.15	0.05
1266	0.000378	0.56	0.25	0.15	0.04
1287	0.000377	0.58	0.24	0.17	0.01

References

- (1) Trinh, M. T.; Houtepen, A. J.; Schins, J. M.; Hanrath, T.; Piris, J.; Knulst, W.; Goossens, A.; Siebbeles, L. D. A. In spite of recent doubts carrier multiplication does occur in PbSe nanocrystals. *Nano Lett.* **2008**, *8*, 1713-1718.
- (2) Weller, A. Photoinduced electron transfer in solution: Exciplex and radical ion pair formation free enthalpies and their solvent dependence. *Z. Phys. Chem.* **1982**, *133*, 93-98.
- (3) Brus, L. E. A simple model for the ionization potential, electron affinity, and aqueous redox potentials of small semiconductor crystallites. *J. Chem. Phys.* **1983**, *79*, 5566-5571.
- (4) Huang, J.; Stockwell, D.; Huang, Z.; Mohler, D. L.; Lian, T. Photoinduced ultrafast electron transfer from CdSe quantum dots to re-bipyridyl complexes. *J. Am. Chem. Soc.* **2008**, *130*, 5632-5633.
- (5) Zhao, X. J.; Kitagawa, T. Solvent effects of 1,4-benzoquinone and its anion radicals probed by resonance raman and absorption spectra and their correlation with redox potentials. *J. Raman Spectr.* **1998**, *29*, 773-780.
- (6) Abe, T. Theoretical estimation of the redox potentials involving organic and inorganic free radicals. *Bull. Chem. Soc. Jpn.* **1994**, *67*, 699-704.

(7) Lifshitz, E.; Dag, I.; Litvitn, I. D. Optically detected magnetic resonance study of electron/hole traps on CdSe quantum dot surfaces. *J. Phys. Chem. B* **1998**, *102*, 9245-9250.

(8) Knutson, J.R.; Beecham, J.M.; Brand, L. Simultaneous analysis of multiple fluorescence decay curves: A global approach. *Chem. Phys. Lett.* **1983**, *102*, 501-507.